Texture evolution in Mg during rolling with a change of deformation path – a modeling approach

Bartosz Sułkowski ID

AGH University of Science and Technology, Department of Non-Ferrous Metals Engineering, Faculty of Non-Ferrous Metals, al. A. Mickiewicza 30, 30-059 Krakow, Poland.

Abstract

The weakening of strong textures in Mg alloys is a crucial factor in obtaining good quality final products that are less anisotropic. Considerable attention has been focused on experiments to find the optimal chemical composition of alloys or processing conditions. However, to reduce time-consuming experiments, texture simulations can help in specifying future research directions. In the present work, the texture evolution in rolled Mg and its alloys was studied using the viscoplastic self-consistent model. The texture simulations presented in the study cover unidirectional rolling, reverse rolling, and cross rolling of Mg and its alloys to check if the change in deformation path has an impact on the activation of non-basal slip systems. The results obtained in the study may help to design the best processing technology and reduce the mechanical anisotropy of magnesium alloys. Slip systems such as basal, prismatic, and pyramidal were taken into consideration. To reflect the effect of alloying elements on hardening, different values for critical resolved shear stress were considered. Pole figures and slip system activity were investigated to understand the texture evolution during rolling as the deformation path changes. It was found that cross rolling may be the most effective processing technology to reduce strong textures during the rolling of Mg alloys. To activate non-basal systems, critical resolved shear stresses and the Schmid factor must be modified. The former can be changed by increasing the processing temperature, proper alloying elements, or change in the strain rate sensitivity; the latter by changing the deformation path.

Keywords: Mg, deformation path, modeling, texture

1. Introduction

Magnesium alloys are widely used in many industries, such as the automotive, space, health, or energy fields (Lopes et al., 2022; Persaud-Sharma & McGoron, 2012; Prasad et al., 2017; Tan & Ramakrishna, 2021). Increasingly, emerging Mg alloys are attracting attention due to their mixture of remarkable properties, such as high specific strength or biotolerance (Mizelli-Ojdanic et al., 2021; Ojdanic et al., 2020; Wang et al., 2017). However, due to the high anisotropy of their mechanical properties, the use of magnesium alloys is limited (Ahn & Seo, 2018; Hutchinson & Barnett, 2010; Kabirian & Khan, 2015; Nie et al., 2020; Sułkowski & Chulist, 2019; Tadano, 2016). One of the main factors that influences mechanical anisotropy is texture (Imandoust & Al-Samman, 2017; Sułkowski, 2021; Zhang et al., 2017). Considerable efforts have been put into reducing strong textures in plastically deformed Mg alloys (Song et al., 2020; Suwas & Gurao, 2008; Suwas & Mondal, 2019). It can be achieved by a combination of processing conditions and the chemical composition of the alloy

(Al-Samman, 2009; Biswas et al., 2010; Bonarski et al., 2010; Solomon et al., 2019; Sułkowski et al., 2020). However, due to the insufficient number of independent slip systems, the formation of strong textures, especially after severe deformation, is still a considerable problem. The activation of non-basal slip systems leads to the weakening of strong textures in hexagonal metals (Hutchinson & Barnett, 2010; Imandoust & Al-Samman, 2017; Nie et al., 2020). To activate these systems, critical resolved shear stress must be modified in such a way that prismatic or pyramidal slip systems are favored. Increasing the processing temperature, selecting the appropriate alloying elements, or modifying the material's strain rate sensitivity usually solves the problem, at least partially.

On the other hand, good results were obtained in methods where the deformation path was changed. In these methods, the activation of non-basal slip systems is achieved by changing the Schmid factor.

Singh & Schwarzer (2005) processed pure Mg in the temperature range of 200–400°C by rolling with the change of deformation path. The effects of unidirectional, reverse, and cross rolling were investigated. It was discovered that the (0001) fiber is formed primarily with the basal pole split toward the rolling direction (RD). However, cross-rolling weakened the basal texture.

The press formability of AZ31 magnesium alloy was investigated by Chino et al. (2006). The alloy was processed by unidirectional rolling, reverse rolling, and cross rolling. The main texture was (0001) fiber with a split toward RD. It was found that in the cases of reverse rolling and cross rolling, the texture was lower than in the case of unidirectional rolling. As a result, the press formability of AZ31 was enhanced.

The effect of cold and warm rolling on microstructure and texture in AZ31 was also studied by Choquechambi-Catorceno et al. (2018). It was found that cross-rolling with a thickness reduction of more than 15% at temperatures above 100°C strongly weakened the initial basal texture.

However, the nature of weakening the (0001) fiber texture during reverse or cross rolling has not been studied to date in the context of modeling and simulations. The use of a viscoplastic self-consistent model (VPSC) is a common approach in studying texture effects in deformed materials. For example, it was successfully used for the prediction of texture evolution during rolling pure Mg and its alloys (Chapuis & Liu, 2019; Chapuis et al., 2016; Wang et al., 2011). It was discovered that activating non-basal slip systems by decreasing the ratio of basal to non-basal critical resolved shear stress is critical for reducing strong basal texture. It can be achieved due to the proper alloying elements or by increasing the tem-

perature (Nie et al., 2020). However, in some cases, the procedures are difficult to implement, or the results are unsatisfactory. From this point of view, the metal processing techniques with the changed deformation path look very promising, especially with the combination of chemical composition and temperature.

In the present study, the texture evolution of Mg during rolling with a change in deformation path was studied using the VPSC model. The slip system activity and texture were investigated to check whether the change in the deformation path activates the non-basal slip systems and leads to texture weakening. There are experimental results showing that the change in the deformation path may lead to texture weakening but the mechanism is not yet well understood (Chino et al., 2006; Choquechambi-Catorceno et al., 2018; Singh & Schwarzer, 2005). The results presented in this study give more insight into the observed phenomena.

2. Experimental procedure

The viscoplastic self-consistent model was used in this study to investigate the evolution of texture during the rolling of magnesium and its alloys as the deformation path changed. The VPSC model is a well-established and mature approach for studying texture evolution in many different materials. In the model, the texture is determined by the change in grain orientation during deformation due to the shear strains in active slip systems. The shear strains are founded by solving the non-linear problem of strain-stress state in a grain described by the equations:

$$\dot{\epsilon}_{ij} = \dot{\gamma}_0^s \sum_{s=1}^{N} \frac{1}{2}(m_{ij}^s + m_{ji}^s)\text{sign}\left(\frac{\sigma_{ij}m_{ij}^s}{\tau_0^s}\right)\left|\frac{\sigma_{ij}m_{ij}^s}{\tau_0^s}\right|^n \quad (1)$$

where: $\dot{\epsilon}_{ij}$ – a crystal deformation rate; $\dot{\gamma}_0^s$ – a reference strain rate; m^s – the Schmid tensor; σ – a stress state; τ_0^s – a critical resolved shear stress of slip system s; n – a strain rate sensitivity;

and:

$$\dot{\gamma}^s = \dot{\gamma}_0\text{sign}\left(\frac{\tau_r^s}{\tau_0^s}\right)\left|\frac{\tau_r^s}{\tau_0^s}\right|^n \quad (2)$$

where: $\dot{\gamma}^s$ – a shear strain rate of a slip system s; τ_r^s – a shear stress which yield a slip system s deformation and can be determined from by the equation:

$$\tau_r^s = \sigma_{ij}m_{ij}^s \quad (3)$$

The $\dot{\gamma}^s$ for all active slip systems are found by choosing the components of σ tensor in such a way that equation (1) is valid. After that, the spin of the crystal-

lite is calculated using the non-symmetric part of the deformation rate tensor:

$$W = \dot{\omega}_{ij} = \dot{\gamma}^s \sum_{s=1}^{N} \frac{1}{2}(m_{ij}^s - m_{ji}^s) \qquad (4)$$

In the next step, the new orientation of crystallite is determined:

$$g' = \dot{\Omega}g \qquad (5)$$

where: g, g' – the grain orientations described by the Euler angles (ϕ_1, Φ, ϕ_2) before and after a change, and $\dot{\Omega}$:

$$\dot{\Omega} = \dot{\beta}_{ij} - \dot{\omega}_{ij} \qquad (6)$$

The $\dot{\beta}_{ij}$ – the spin of the sample.

Table 1 presents the slip systems taken into consideration in the present study.

Table 1. The slip systems

Slip system	Designation	Slip plane	Slip direction	Burgers vector
Basal	B	(0001)	$\langle 11\bar{2}0 \rangle$	<a>
Prismatic	P	$\{10\bar{1}0\}$	$\langle 1\bar{2}10 \rangle$	<a>
Pyramidal 2nd order	$\pi2$	$\{11\bar{2}2\}$	$\langle 11\bar{2}3 \rangle$	<a + c>

Table 2 presents the values of critical resolved shear stress (τ_0^s) and strain rate sensitivity (n) for considered slip systems presented in Table 1. The values were chosen based on the literature review (Chapuis & Liu, 2019; Chapuis et al., 2016; Hutchinson & Barnett, 2010; Nie et al., 2020). The values reflect the increase in τ_0^s due to the hardening from alloying elements in Mg alloys.

Table 2. Variants of simulations in the first stage with the parameters used in the model (Chapuis & Liu, 2019; Chapuis et al., 2016; Hutchinson & Barnett, 2010; Nie et al., 2020)

Simulation variant	ϵ	Slip system	τ_0^s [MPa]	n	$\tau_0^{P,\pi2}/\tau_0^B$
R1	0.3	B	1	0.05	–
		P	45	0.08	45
		$\pi2$	55	0.1	55
R2	0.3	B	3	0.08	–
		P	60	0.15	20
		$\pi2$	75	0.18	25

The simulation procedure was as described below. First, there were two rolling simulation variants labeled R1 and R2. Variant R1 reflects the rolling of pure Mg where the τ_0^s for non-basal slip systems (P and $\pi2$) are very high. On the other hand, in variant R2, the τ_0^s for the slip systems are increased to reflect the influence of the alloying elements in Mg alloys. However, despite the fact that the τ_0^s for the individual slip system is increased, the overall ratio $\tau_0^{P,\pi2}/\tau_0^B$ is reduced making the activation of non-basal slip systems more favorable.

The texture evolution for the initial material started with the random texture. The deformation equal to $\epsilon = 0.3$ was applied. These were the simulated variants R1 and R2. That was the first stage of deformation. Then, there was another stage of simulations, after the rolling direction was rotated around the normal direction. In this stage, an additional deformation equal to $\epsilon = 0.3$ was applied, so the total deformation was equal to $\epsilon = 0.6$. The starting texture in the second stage of simulations came from the first step of simulations. During the second stage of deformation, the rolling direction of the first stage was rotated clockwise around the normal plane direction (ND) by a certain degree. In the variant of unidirectional rolling (UR), the rotation was equal to 0° to reflect continuous rolling. Next, in the variant cross-rolling (CR), the rotation was equal to 90°, and finally, in the variant reverse-rolling (RR), the rotation was equal to 180°. Table 3 summarizes all of the investigated variants and rotations. The parameters shown in Table 2 were used during modeling in the second stage of simulations.

Table 3. The summary of the simulation variants during the second stage of deformation with the degree of rotation around ND

Variant	Process	Clockwise rotation around ND	Additional ϵ	Total ϵ
R1-UR	unidirectional rolling	0°	0.3	0.6
R1-CR	cross rolling	90°	0.3	0.6
R1-RR	reverse rolling	180°	0.3	0.6
R2-UR	unidirectional rolling	0°	0.3	0.6
R2-CR	cross rolling	90°	0.3	0.6
R2-RR	reverse rolling	180°	0.3	0.6

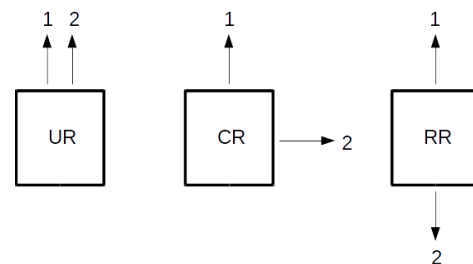Figure 1 shows the sketch depicting the deformation scheme.

Fig. 1. The sketch showing the deformation scheme during rolling with the change in deformation path: 1 – rolling in the first stage; 2 – rolling in the second stage

3. Results

The pole figures (0001), {10$\bar{1}$0}, and ⟨11$\bar{2}$0⟩ of simulated rolling textures for variants R1 and R2 are presented in Figure 2.

From Figure 2, it is seen that the texture for variant R1 is a type of the (0001) fiber with the maximum intensity around c direction. This kind of texture is typical for rolling pure magnesium (Hutchinson & Barnett, 2010; Nie et al., 2020; Tadano, 2016). This is due to the significant difference in critical resolved shear stresses (CRSS) between basal and non-basal slip systems. In the case of variant R2, where the differences in CRSS are much smaller, the texture changed. There are observed two picks of intensity split toward RD. This is typical for rolled Mg alloys (Hutchinson & Barnett, 2010; Imandoust & Al-Samman, 2017; Nie et al., 2020).

Figure 3 shows the slip system activity during the simulation of the rolling texture in the variants R1 and R2.

Comparing Figure 2, Figure 3, and the data in Table 3, it is clear that the (0001) fiber texture is a result of the dominance of the B slip system due to the lowest CRSS. However, when the ratio of CRSS between P, π2 and B slip systems is lowered, as in the case of magnesium alloys, the activity of non-basal slip systems is much larger. This has an effect on the splitting of the (0001) fiber peak into two toward RD.

The pole figures (0001), {10$\bar{1}$0}, and ⟨11$\bar{2}$0⟩ of the simulated rolling textures for the variants R1 followed by unidirectional rolling, cross rolling and reverse rolling are shown in Figure 4. It is seen that in the case of this variant, the (0001) fiber texture was strengthened despite the deformation scheme. The corresponding slip system slip system activity is shown in Figure 5. It can be observed that in all the variants, the slip activity for the B slip systems is the highest. This is the result of the lowest CRSS for that slip system.
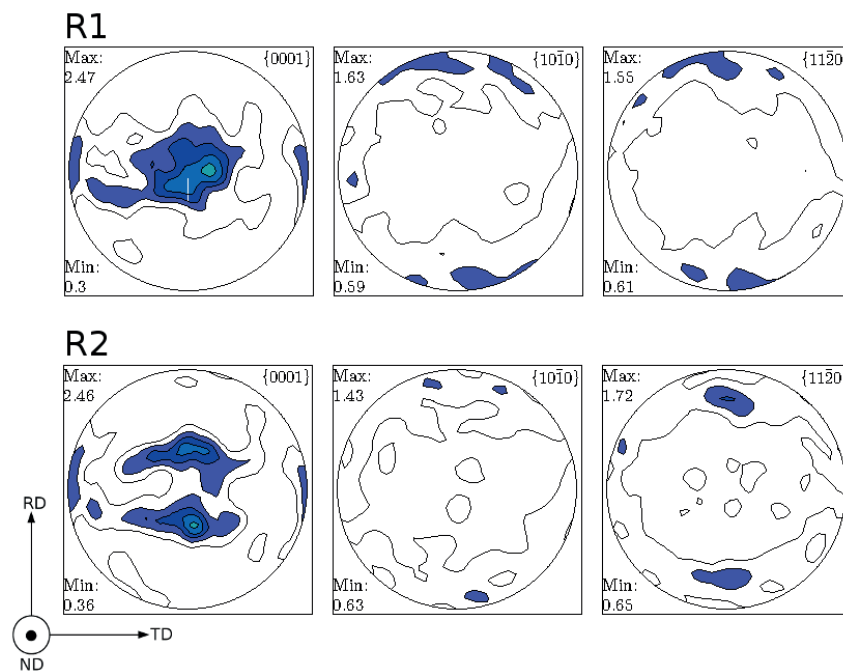

Fig. 2. Pole figures (0001), {10$\bar{1}$0}, and ⟨11$\bar{2}$0⟩ of R1 and R2 variants of the simulated rolling textures
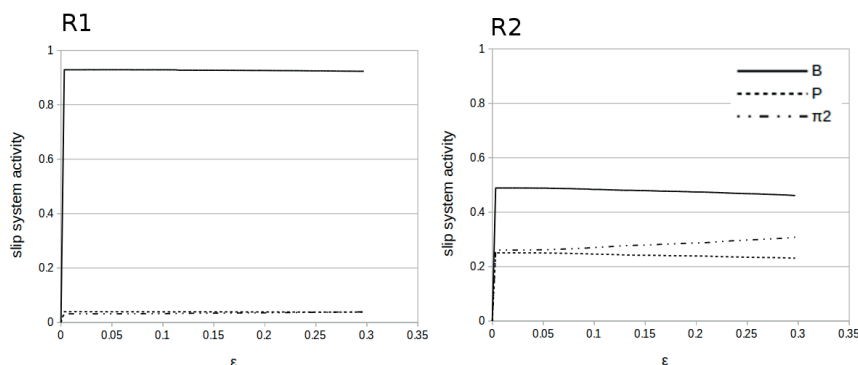

Fig. 3. Slip system activity of the simulated rolling textures for the variants R1 and R2
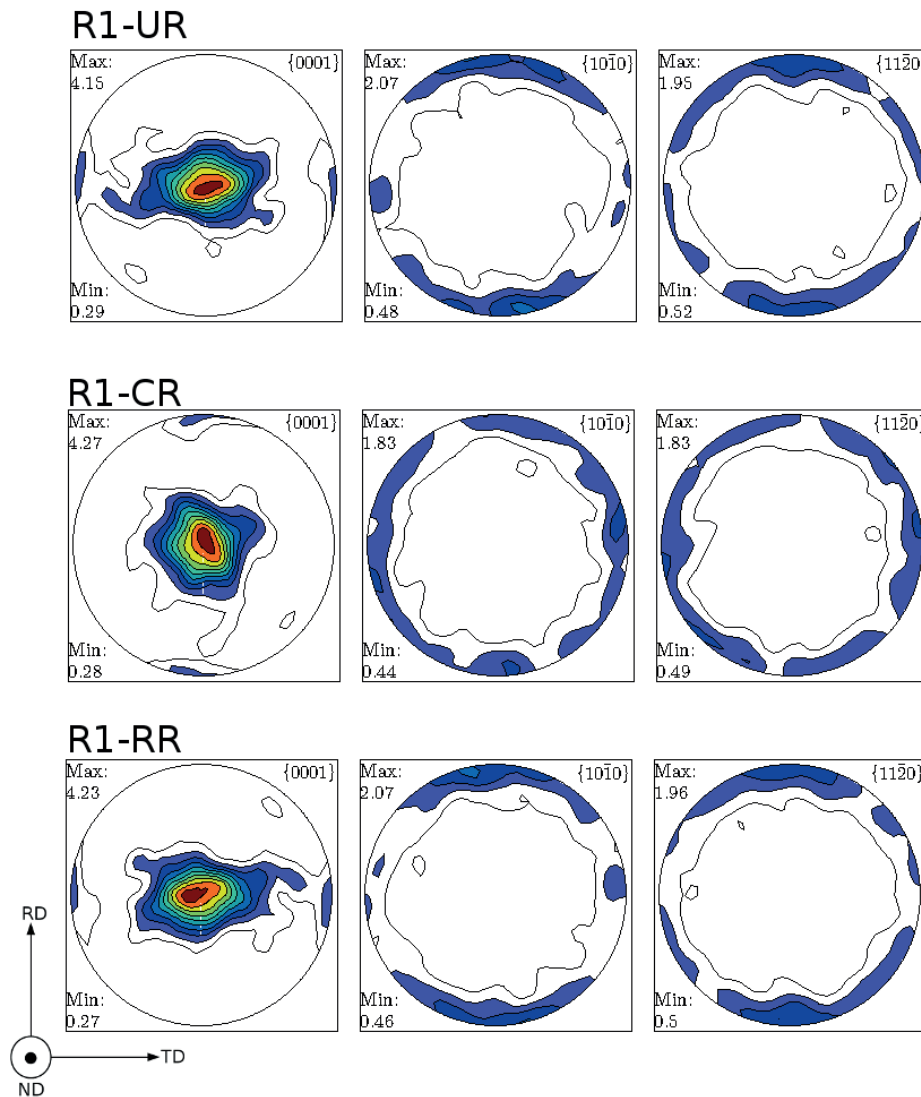
R1-UR

R1-CR

R1-RR

Fig. 4. Pole figures (0001), {10$\bar{1}$0}, and ⟨11$\bar{2}$0⟩ of the simulated variants R1-UR, R1-CR and R1-RR
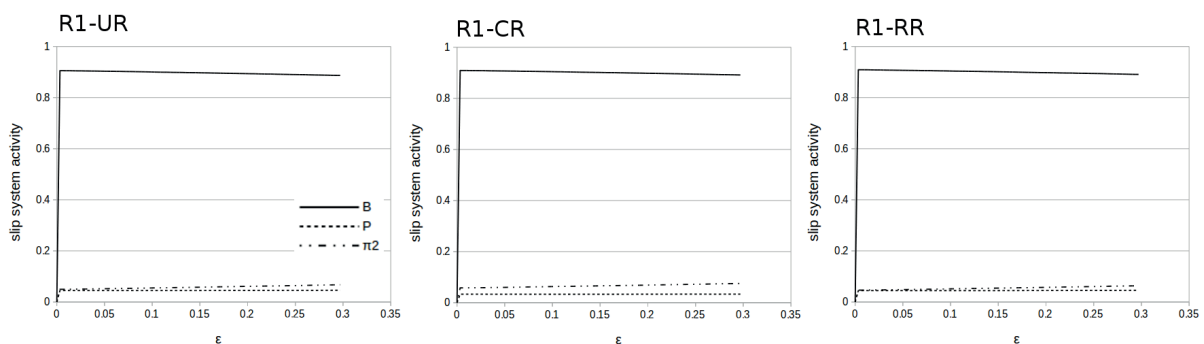

Fig. 5. Slip system activity of the simulated rolling textures for the variants R1-UR, R1-CR and R1-RR

The simulated pole figures (0001), {10$\bar{1}$0}, and ⟨11$\bar{2}$0⟩ for the variants R2 followed by the unidirectional rolling, cross rolling and reverse rolling are shown in Figure 6. It is seen that in the case of the variants R2-UD and R2-RR the texture was much stronger than in the variant R2. However, in the case of the variant R2-CR, the texture changed in such a way that now the intensity peaks are shifted toward TD. This is the result of the change in the deformation path while the RD was rotating clockwise by 90° around the ND. Moreover, it can be seen that the texture is much weaker than the texture in the variants R2-UD and R2-RR.

The corresponding slip system activity for the variants R2-UR, R2-CR and R2-RR is shown in Figure 7. It can be seen that the slip system activity for the P and π2 slip systems is at a very similar level as that for the B slip system. As a result, the texture is much weaker than the texture in the variants R1-UR, R1-CR, and R1-RR. Moreover, in the case of R2-CR, there is a change in the main slip system from B to π2. This change is responsible for hindering texture evolution in the variant R2-CR.
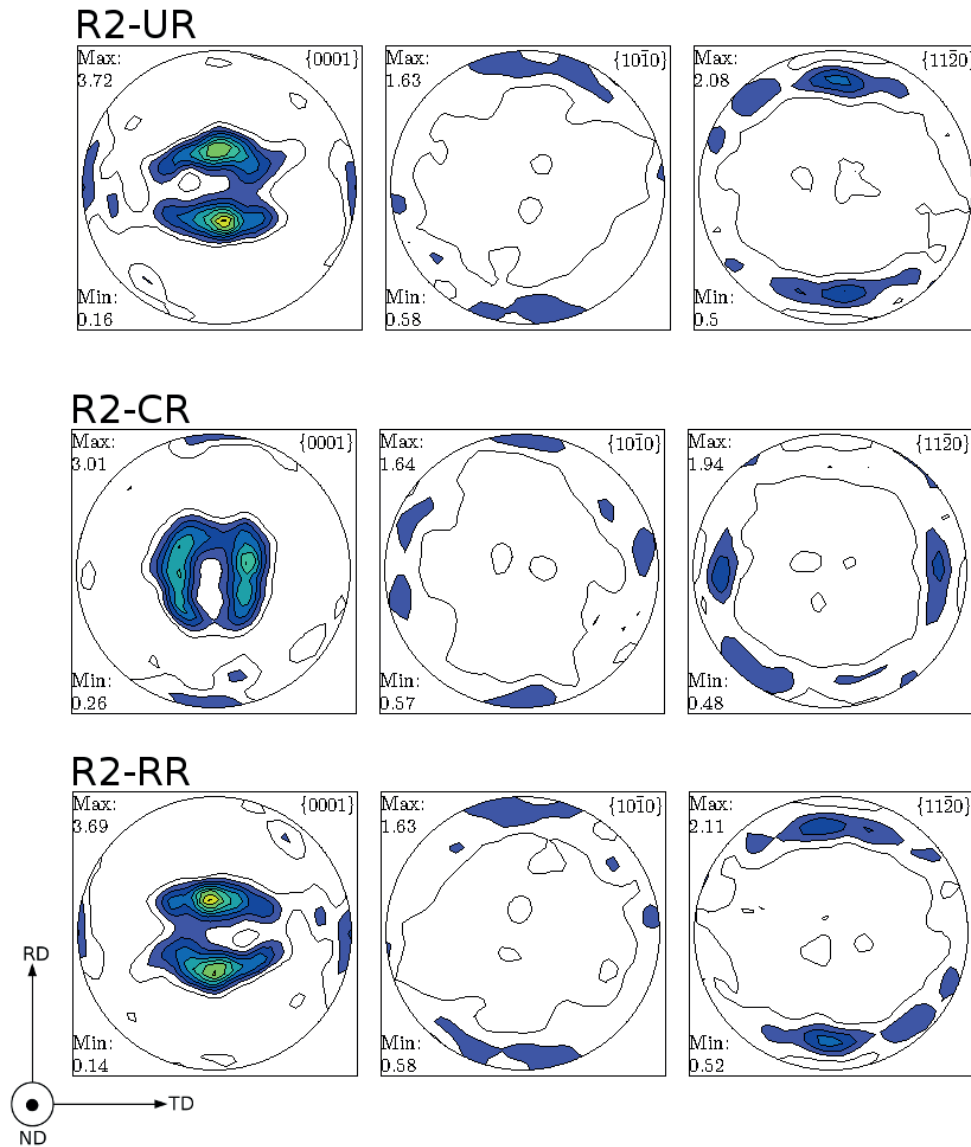

Fig. 6. Pole figures (0001), {10$\bar{1}$0}, and ⟨11$\bar{2}$0⟩ of the simulated variants R2-UR, R2-CR and R2-RR
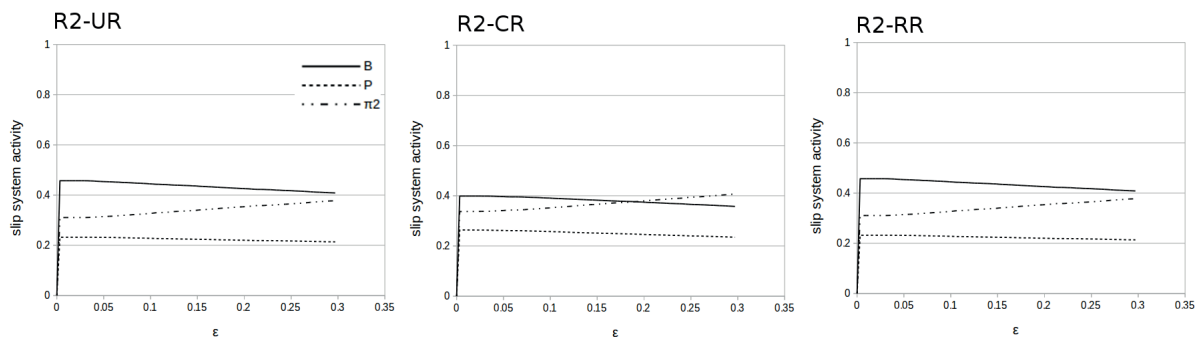

Fig. 7. Slip system activity of the simulated rolling textures for the variants R2-UR, R2-CR and R2-RR

4. Discussion

In the present study, texture weakening was observed during simulations of cross-rolling when the main component was (0001) basal with a split toward RD. This was also observed during the experiments of rolled Mg and its alloys (Chino et al., 2006; Choquechambi--Catorceno et al., 2018; Singh & Schwarzer, 2005). The presented results provide more information about the slip system activity during Mg deformation as the deformation path changes. The simulations show that two mechanisms overlap in this case.

The first mechanism is the weakening of texture due to the splitting of the basal component. That effect is observed in many Mg alloys, especially in the Mg-RE (rare elements) alloys (Imandoust & Al-Samman, 2017; Nie et al., 2020). The slip of the basal component takes place toward RD, and the range of the split depends on the alloying element, however, it is usually about 5–15°. Alloying elements change the CRSS for a particular slip system; however, in Mg single crystals, Zn can increase the CRSS for the B slip system while decreasing the CRSS for the P slip system at the same time (Akhtar & Teghtsoonian, 1969a, 1969b, 1972). On the other hand, the high temperature during processing strongly reduces CRSS for the P and $\pi2$ systems while only slightly influencing CRSS for the B system (Britton et al., 2015; Nie et al., 2020). This leads to a decrease in the ratio of the basal CRSS to the non-basal CRSS and increases the activity of the P and $\pi2$ systems. Comparing Figures 4 and 6, this effect is clearly seen. The weakening is associated with higher non-basal slip system activity than in the case of UR or RR.

The favorable Schmid factor for non-basal slip systems is the second mechanism responsible for weakening the texture during the variant R2-CR. Nan et al. (2012, 2013) calculated Schmid factors in a wide range of orientations and slip systems for many hexagonal metals. It was shown that for the orientation along the *c* axis, the Schmid factor for the B system is very low, while

for the P and $\pi2$, is very high. The maximum value of the Schmid factor for the non-basal slip system is for the orientation around 15° out of the *c* axis. This corresponds very well with the typical angle for splitting the basal component in Mg alloys during rolling. While there is a change in the deformation path in the case of the variant R2-CR, the maxima are 15° toward TD (see Fig. 6). During the cross-rolling, the texture changes. The peaks split toward RD, and this leads to texture weakening.

5. Conclusions

To sum up, the variant R2-CR was the most effective rolling method for hampering strong texture evolution during the rolling of Mg and its alloys. This was achieved by two mechanisms. The first mechanism was the splitting of the basal component toward RD. The second mechanism was the increase in slip system activity of non-basal slip systems due to the change in deformation path by means of the favorable Schmid factor.

The findings of this study contribute to a better understanding of the texture evolution in magnesium and its alloys. However, more experiments are needed to elaborate on the effects of different alloying elements, such as RE. Moreover, the effects of temperature and dynamic recrystallization processes must be studied experimentally and by simulations. Nevertheless, the results obtained show that the activation of the non-basal slip system due to the change in deformation path can lead to texture weakening in Mg alloys.

Acknowledge

References

Akhtar, A., & Teghtsoonian, E. (1969a). Solid solution strengthening of magnesium single crystals – I alloying behaviour in basal slip. *Acta Metallurgica*, *17*(11), 1339–1349. https://doi.org/10.1016/0001-6160(69)90151-5.

Akhtar, A., & Teghtsoonian, E. (1969b). Solid solution strengthening of magnesium single crystals – II the effect of solute on the ease of prismatic slip. *Acta Metallurgica*, *17*(11), 1351–1356. https://doi.org/10.1016/0001-6160(69)90152-7.

Akhtar, A., & Teghshoonian, E. (1972). Substitutional solution hardening of magnesium single crystals. *The Philosophical Magazine: A Journal of Theoretical Experimental and Applied Physics*, *25*(4), 897–916. https://doi.org/10.1080/14786437208229311.

Al-Samman, T. (2009). Comparative study of the deformation behavior of hexagonal magnesium-lithium alloys and a conventional magnesium AZ31 alloy. *Acta Materialia*, *57*(7), 2229–2242. https://doi.org/10.1016/j.actamat.2009.01.031.

Biswas, S., Dhinwal, S.S., & Suwas, S. (2010). Room-temperature equal channel angular extrusion of pure magnesium. *Acta Materialia*, *58*(9), 3247–3261. https://doi.org/10.1016/j.actamat.2010.01.051.

Bonarski, B.J., Schafler, E., Mikulowski, B., & Zehetbauer, M.J. (2010). Effects of recrystallization on texture, microstructure and mechanical properties in HPT-deformed pure Mg. *Journal of Physics: Conference Series*, 240, 012133, https://doi.org/10.1088/1742-6596/240/1/012133.

Britton, T.B., Dunne, F.P.E., & Wilkinson, A.J. (2015). On the mechanistic basis of deformation at the microscale in hexagonal close-packed metals. *Proceedings of the Royal Society A*, *471*(2178). https://doi.org/10.1098/rspa.2014.0881.

Chapuis, A., & Liu, Q. (2019). Modeling strain rate sensitivity and high temperature deformation of Mg-3Al-1Zn alloy. *Journal of Magnesium and Alloys*, *7*(3), 433–443. https://doi.org/10.1016/j.jma.2019.04.004.

Chapuis, A., Wang, Z., & Liu, Q. (2016). Influence of material parameters on modeling plastic deformation of Mg alloys. *Materials Science & Engineering: A*, *655*, 244–250, https://doi.org/10.1016/j.msea.2015.12.067.

Chino, Y., Sassa, K., Kamiya, A., & Mabuchi, M. (2006). Influence of rolling routes on press formability of a rolled AZ31 Mg alloy sheet. *Materials Transactions*, *47*(10), 2555–2560. https://doi.org/10.2320/matertrans.47.2555.

Choquechambi Catorceno, L.L., Abreu, H.F.G., de, & Padhila, A.F. (2018). Effects of cold and warm cross-rolling on microstructure and texture evolution of AZ31B magnesium alloy sheet. *Journal of Magnesium and Alloys*, *6*(2), 121–133. https://doi.org/10.1016/j.jma.2018.04.004.

Hutchinson, W.B., & Barnett, M.R. (2010). Effective values of critical resolved shear stress for slip in polycrystalline magnesium and other hcp metals. *Scripta Materialia*, *63*(7), 737–740. https://doi.org/10.1016/j.scriptamat.2010.05.047.

Imandoust, A., Barrett, C.D., & Al-Samman, T., Inal, K.A., El Kadiri, A. (2017). A review on the effect of rare-earth elements on texture evolution during processing of magnesium alloys. *Journal of Materials Science*, *52*(1), 1–29. https://doi.org/10.1007/s10853-016-0371-0.

Kabirian, K., & Khan, A.S. (2015). Anisotropic yield criteria in r–s stress space for materials with yield asymmetry. *International Journal of Solids and Structures*, *67–68*, 116–126. https://doi.org/10.1016/j.ijsolstr.2015.04.006

Kanghwan, A., & Min-Hong, S. (2018). Effect of anisotropy and differential work hardening on the failure prediction of AZ31B magnesium sheet at room temperature. *International Journal of Solids and Structures*, *138*, 181–192. https://doi.org/10.1016/j.ijsolstr.2018.01.011.

Lopes, V., Puga, H., Gomes, I.V., Peixinho, N., Teixeira, J.C., & Barbosa, J. (2022). Magnesium stents manufacturing: Experimental application of a novel hybrid thin-walled investment casting approach. *Journal of Materials Processing Technology*, *299*, 117339. https://doi.org/10.1016/j.jmatprotec.2021.117339.

Mizelli-Ojdanic, A., Horky, J., Mingler, B., Fanetti, M., Gardonio, S., Valant, M., Sułkowski, B., Schafler, E., Orlov, D., & Zehetbauer, M.J. (2021). Enhancing the mechanical properties of biodegradable Mg alloys processed by warm HPT and thermal treatments. *Materials*, *14*(21), 6399. https://doi.org/10.3390/ma14216399.

Nan, X.-L., Wang, H.-Y., Zhang, L., Li, J.-B., & Jiang, Q.-Ch. (2012). Calculation of Schmid factors in magnesium: Analysis of deformation behaviors. *Scripta Materialia*, *67*(5), 443–446, https://doi.org/10.1016/j.scriptamat.2012.05.042.

Nan, X.-L., Wang, H.-Y., Wu, Z.-Q., Xue, E.-S., Zhang, L., & Jiang, Q.-Ch. (2013). Effect of c/a axial ratio on Schmid factors in hexagonal close-packed metals. *Scripta Materialia*, *68*(7), 530–533, https://doi.org/10.1016/j.scriptamat.2012.12.006.

Nie, J.F., Shin, K.S., & Zeng, Z.R. (2020). Microstructure, deformation, and property of wrought magnesium alloys. *Metallurgical and Materials Transactions A*, *51*(12), 6045–6109. https://doi.org/10.1007/s11661-020-05974-z.

Ojdanic, A., Horky, J., Mingler, B., Fanetti, M., Gardonio, S., Valant, M., Sułkowski, B., Schafler, E., Orlov, D., & Zehetbauer, M.J. (2020). The effects of severe plastic deformation and/or thermal treatment on the mechanical properties of biodegradable Mg-Alloys. *Metals*, *10*(8), 1064, https://doi.org/10.3390/met10081064.

Persaud-Sharma, D., & McGoron, A. (2012). Biodegradable magnesium alloys: A review of material development and applications. *Journal of Biomimetics, Biomaterials and Tissue Engineering*, *3*, 25–39. https://doi.org/10.4028/www.scientific.net/JBBTE.12.25.

Prasad, K., Bazaka, O., Chua, M., Rochford, M., Fedrick, L., Spoor, J., Symes, R., Tieppo, M., Collins, C., Cao, A., Markwell, D., Ostrikov, K., & Bazaka, K. (2017). Metallic biomaterials: current challenges and opportunities. *Materials*, *10*(8), 884. https://doi.org/10.3390/ma10080884.

Singh, A.K., & Schwarzer, R.A. (2005). Evolution of texture in pure magnesium during rolling. *Zeitschrift für Metallkunde*, *96*(4), 345–351.

Solomon, E.L.S., Natarajan, A.R., Roy, A.M., Sundararaghavan, V., Van der Ven, A., & Marquis, E.A. (2019). Stability and strain-driven evolution of β′ precipitate in Mg-Y alloys. *Acta Materialia*, *166*, 148–157, https://doi.org/10.1016/j.actamat.2018.12.026.

Song, J., She, J., Chen, D., & Pan, F. (2020). Latest research advances on magnesium and magnesium alloys worldwide. *Journal of Magnesium and Alloys*, *8*(1), 1–41. https://doi.org/10.1016/j.jma.2020.02.003.

Sułkowski, B. (2021). The effect of structure and texture on pure magnesium properties. *International Journal of Materials Research*, *112*(1), 57–62, https://doi.org/10.1515/ijmr-2020-7815.

Sułkowski, B., & Chulist, R. (2019). Twin-induced stability and mechanical properties of pure magnesium. *Materials Science and Engineering: A*, *749*, 89–95. https://doi.org/10.1016/j.msea.2019.01.118.

Sułkowski, B., Janoska, M., Boczkal, G., Chulist, R., Mroczkowski, M., & Pałka, P. (2020). The effect of severe plastic deformation on the Mg properties after CEC deformation. *Journal of Magnesium and Alloys*, *8*(3), 761–768. https://doi.org/10.1016/j.jma.2020.04.005.

Suwas, S., & Gurao, N.P. (2008). Crystallographic texture in materials. *Journal of the Indian Institute of Science*, *88*(2), 151–177.

Suwas, S., & Mondal, S. (2019). Texture evolution in severe plastic deformation processes. *Materials Transactions*, *60*(8), 1457–1471. https://doi.org/10.2320/matertrans.MF201933.

Tadano, Y. (2016). Formability of magnesium sheet with rolling texture. *International Journal of Mechanical Sciences*, *108–109*, 72–82, https://doi.org/10.1016/j.ijmecsci.2016.01.031.

Tan, J., & Ramakrishna, S. (2021). Applications of magnesium and its alloys: A review. *Applied Sciences*, *11*(15), 6861. https://doi.org/10.3390/app11156861.

Wang, H., Wu, P.D., Boyle, K.P., & Neale, K.W. (2011). On crystal plasticity formability analysis for magnesium alloy sheets. *International Journal of Solids and Structures*, *48*, 1000–1010. https://doi.org/10.1016/j.ijsolstr.2010.12.004.

Wang, L., Jiang, J., Ma, A., Li, Y., & Song, D. (2017). Critical review of Mg-based hydrogen storage materials processed by equal channel angular pressing. *Metals*, *7*(9), 324. https://doi.org/10.3390/met7090324.

Zeng, Z., Nie, J.F., Xu, S.-W., Davies, Ch.H.J., & Birbilis, N. (2017). Super-formable pure magnesium at room temperature. *Nature Communications*, *8*, 972. https://doi.org/10.1038/s41467-017-01330-9.

Zhang, H., Huang, G., Kong, D., Sang, G., & Song, B. (2011). Influence of initial texture on formability of AZ31B magnesium alloy sheets at different temperatures. *Journal of Materials Processing Technology*, *211*(10), 1575–1580. https://doi.org/10.1016/j.jmatprotec.2011.04.009.